Asian Journal of Chemistry; Vol. 36, No. 1 (2024), 206-214

ASIAN JOURNAL OF CHEMISTRY

https://doi.org/10.14233/ajchem.2024.28284

# Adsorption of Lead(II) from Aqueous Solution by Synthetic Barium Hexaferrite Magnetic Nanoparticles

PARINTIP RATTANABURI[1], PAWEENA PORRAWATKUL[2], RUNGNAPA PIMSEN[2] and PRAWIT NUENGMATCHA[1,2,*]

[1]Creative Innovation in Science and Technology, Faculty of Science and Technology, Nakhon Si Thammarat Rajabhat University, Nakhon Si Thammarat 80280, Thailand
[2]Nanomaterials Chemistry Research Unit, Department of Chemistry, Faculty of Science and Technology, Nakhon Si Thammarat Rajabhat University, Nakhon Si Thammarat 80280, Thailand

*Corresponding author: Tel/Fax: +66 7 5377443; E-mail: pnuengmatcha@gmail.com

*Received*: 2 August 2023; *Accepted*: 2 December 2023; *Published online*: 31 December 2023; AJC-21505

In this study, the sol-gel auto-combustion method is employed to synthesize barium hexaferrite ($BaFe_{12}O_{19}$) using carboxymethyl cellulose as chelating agent. The properties and identity of the synthesized $BaFe_{12}O_{19}$ nanoparticles were verified with X-ray diffraction (XRD), scanning electron microscopy (SEM), Fourier-transform infrared spectroscopy (FTIR), energy dispersive spectroscopy (EDS) and vibrating sample magnetometry (VSM). The adsorption efficiency of the prepared nanoparticles toward lead(II) metal ions was estimated using atomic absorption spectroscopy (AAS). The synthesized $BaFe_{12}O_{19}$ was utilized as an adsorbent for removing lead(II) from the aqueous solution. The utilization enhancement studies of the synthesized nanoparticles were influenced by several factors, which include incubation time, pH of metal ion solutions, adsorbent doses, initial lead(II) metal ion concentration and temperature. Under optimum conditions, when 0.20 g of adsorbent was used with 5 mg/L of lead(II) ion solution at a pH 6, the adsorption percentage was found to be 91.53%. Endothermic adsorption and the Langmuir isotherm models were found to best fit the data of lead(II) adsorption. Notably, the maximum adsorption capacity ($q_m$) for lead adsorption was 4.57 mg/g. These findings demonstrated that the novel single material $BaFe_{12}O_{19}$ magnetic nanoparticles can function as a highly effective nanosorbent for the treatment of wastewater and they can effectively remove lead(II) ions.

**Keywords: Barium hexaferrite, Adsorbent, Magnetic nanoparticles, Lead heavy metal, Nanosorbent.**

## INTRODUCTION

Water pollution is one of the most pressing global concerns as the world faces a future with declining water resources [1]. Heavy metals in water originate from various sources, including those caused by humans as well as by natural processes [2]. These heavy metals eventually make their way into the bodies of animals and humans through the food chain due to their absorption by plants, where they have a deleterious impact on health and vitality [3]. The release of untreated or minimally treated heavy metals into waterways has several adverse effects on human health and the environment. Heavy metals are particularly harmful to humans because of their great stability and solubility in water. Heavy metal contaminants have numerous adverse impacts on the environment and human health because of their high reactivity, propensity to form complexes and high biochemical and physiological activity [4]. According to the World Health Organization [5], heavy metals become toxic at concentrations greater than 1 mg/L. Lead causes cerebral, renal, circulatory and nervous disorders when its concentration is $6.0 \times 10^{-3}$ mg/L, which corresponds to the maximum contaminant level (MCL) standards for harmful heavy metals [6]. Lead is typically released into the environment by the metal mining industry. The production of acid lead batteries [7], agricultural wastewater discharge, domestic sewage discharge and atmospheric deposition all contribute to lead pollution [8]. Lead is a non-biodegradable metal that exists in nature in low quantities. However, atmospheric lead levels are steadily rising because of human activities such as manufacturing, mining and the burning of fossil fuels. Lead is toxic to the human body when exposed to amounts exceeding the optimum range and children, in particular, are vulnerable to lead poisoning because of their increased likelihood of coming into contact with dust containing environmental lead [9]. Therefore, wastewater contaminated

with heavy metals must be treated before being released into the environment to prevent unintended consequences, such as contamination of drinking water supplies. Numerous techniques, which include coagulation, chemical precipitation, membrane filtration, ion exchange and biosorption [10-12], have been developed to reduce heavy metal pollution in water. Most of these methods are not sustainable because of some challenges involved, such as additional pollution, high energy consumption, high costs and complex processes. The adsorption process is a low-cost technique to remove heavy metals from polluted fluids [13]. Adsorption is classified as either physical, in which non-specific van der Waals forces cause an increase in the adsorbate concentration at the interface or chemisorption, where covalent or ionic bonds are formed between the adsorbate and the adsorbent. Unlike chemisorption, which is selective, typically irreversible and generates heat in the range of tens to hundreds of kJ/mol, physical adsorption is only weakly specific, reversible and thermally effective [14].

The search for a cost-effective adsorbent that has high stability and is highly effective continues. These adsorbents are often prepared from porous materials, which gives them a high surface area. Therefore, the synthesis of an adsorbent with a large surface area and low diffusion resistance is crucial to environmental remediation. Thus far, extensive research has been conducted on the use of magnetic nanomaterials in water purification. Several studies have demonstrated the effectiveness of magnetic nanomaterials in water purification by removing organic, inorganic and heavy metal contaminants [15]. Magnetic nanosorbents are potential options for the removal of heavy metals in the presence of an external magnetic field because of their high efficiency, low cost, flexibility of adsorption process, high specific surface area, facile synthesis methods and high adsorption and desorption properties [16]. In a previous studies [17,18], magnetic adsorbents such as magnetic nanobiocomposite, magnetic polyresorcinol@$CoFe_2O_4$@MnS nanoparticles, amino/thiol bifunctionalized magnetic nanoadsorbent, nano metal ferrites-$MFe_2O_4$ and DMSA@$SiO_2$@$Fe_3O_4$ nanocomposite were investigated for heavy metal adsorption processes.

Barium hexaferrite ($BaFe_{12}O_{19}$) is a permanent magnet that has numerous applications in magnetic nanomaterial technology, making it an important material class within the family of permanent magnets [19]. $BaFe_{12}O_{19}$ can be rapidly and easily separated from the solution due to its high magnetocrystalline anisotropy and high coercivity [20]. These nanomaterials are effective as adsorbents due to their high surface area and pore volume and have piqued commercial interest [21]. Various methods including the sol-gel technique were utilized for the synthesis of $BaFe_{12}O_{19}$ magnetic nanoparticles [22]. In previous study, the sol-gel auto-combustion method was used to successfully synthesize $BaFe_{12}O_{19}$, resulting in the formation of single-phase barium hexaferrite at low cost [23]. Various new approaches have been developed in recent years to remove heavy metals from the wastewater produced by industrial processes. Due to several advantageous characteristics of $BaFe_{12}O_{19}$, it is being utilized in several new applications in the adsorption process. In this study, $BaFe_{12}O_{19}$ nanoparticles were synthesized *via* the sol-gel auto-combustion method using carboxymethyl cellulose as a chelating agent for removing lead(II) ions present in an aqueous solution. Additionally, the various factors that impact the efficiency of adsorbents in removing heavy metals from wastewater were also studied. These factors include incubation time, pH value, adsorbent dose, initial concentration and temperature. The removal efficiency of heavy metals was estimated using atomic absorption spectroscopy (AAS). The adsorptive behaviour of the $BaFe_{12}O_{19}$ adsorbent was analyzed *via* isotherm and thermodynamic experiments.

## EXPERIMENTAL

All the chemical reagents used in the experiment were of analytical grade and used as received. Iron(III) nitrate nonahydrate [$Fe(NO_3)_3{\cdot}9H_2O$], barium(II) nitrate [$Ba(NO_3)_2$], carboxymethyl cellulose and lead(II) nitrate nonahydrate [$Pb(NO_3)_2{\cdot}9H_2O$] were purchased from Sigma-Aldrich, USA. Nitric acid (65% $HNO_3$), sodium acetate and ammonium hydroxide (28-30%) were purchased from Baker, U.K.

### Preparation and characterization of $BaFe_{12}O_{19}$ magnetic nanoparticle adsorbent

The adsorbent magnetic nanoparticle, barium hexaferrite ($BaFe_{12}O_{19}$), was prepared by reported techniques [24]. $BaFe_{12}O_{19}$ was prepared by mixing 0.26 g of barium(II) nitrate and 4.85 g of iron(III) nitrate in 50 mL of distilled water. Both solutions were mixed and continuously stirred for 30 min. Then, 6% (w/v) carboxymethyl cellulose was added as a chelating agent to the above solution while stirring. After heating the mixture to 80 ºC, $NH_4OH$ (30% v/v) was slowly added until the mixture attained a highly alkaline pH (pH = 10). To remove the solvent and set the gel, the resulting solution was stirred for 2 h at 90 ºC and then at 200 ºC. The dried gel swelled on ignition. Besides, the gel completely self-combusted within a minute, resulting in a black powder. The crystal structure was characterized using the X-ray diffraction (XRD) technique (Shimata, XD-D1, Japan) and the phase of the synthesized $BaFe_{12}O_{19}$ was characterized by a diffractometer (source: Cu$K_\alpha$ radiation). The sample was analyzed using the scanning electron microscopy-energy dispersion spectroscopy (SEM-EDS) technique with a Quanta 400 (SEM-Quanta) system. The Fourier-transform infrared (FTIR) spectrum of barium hexaferrite ($BaFe_{12}O_{19}$) magnetic nanoparticles was recorded on a Nicolet iS5 spectrometer from Thermo-Scientific. The measurements were taken using the KBr pellet method at room temperature in the wavelength range of 4000-500 $cm^{-1}$. The specific surface area (Autosorb iQ S/N:1050017338 Station: 2) was calculated using the Brunauer-Emmet-Teller (BET) method. The magnetization of the $BaFe_{12}O_{19}$ samples was measured using the vibrating sample magnetometry (VSM) (Lake Shore; Model 7404) technique in the range of -12 kOe to 12 kOe at room temperature.

**Preparation of stock solution of Pb(II) ion:** To prepare a stock solution of Pb(II) with a concentration of 100 mg/L, 100 mg of $Pb(NO_3)_2{\cdot}9H_2O$ was dissolved in 1000 mL volumetric flask using 1% $HNO_3$ as solvent. The experimental solutions of 1, 5, 10, 15, 20, 25 and 30 mg/L were prepared by sequentially diluting the stock solution. A series of dilutions of the

standard stock solution were prepared at concentrations of 1, 5, 10, 20 and 30 mg/L for a standard calibration curve.

**Adsorption of Pb(II) ions on $BaFe_{12}O_{19}$ magnetic nanoparticle adsorbent:** The adsorption efficiency of Pb(II) on $BaFe_{12}O_{19}$ magnetic nanoparticle adsorbent was established through batch experiments. Moreover, several factors that affect the efficiency of adsorption were considered and batch adsorption experiments were conducted. In each batch experiment, the adsorbent $BaFe_{12}O_{19}$ was weighed and added to a 125 mL Erlenmeyer flask and 25 mL of Pb(II) solution was subsequently added. The prepared solution was shaken with an orbital shaker with a speed of 150 rpm after its pH was adjusted. The impact of the following parameters of the experiment on the removal of Pb(II) from aqueous solution was investigated: incubation time (10, 20, 30, 40, 50, 60 and 90 min), pH value of solution (1, 2, 3, 4, 5, 6 and 7), adsorbent dose (0.02, 0.04, 0.08, 0.12, 0.16 and 0.20 g), initial concentration of Pb(II) (1, 5, 10, 15, 20, 25 and 30 mg/L) and temperature (10, 30 and 50 ºC). The suspension of $BaFe_{12}O_{19}$ adsorbent was separated from Pb(II) using an external magnet and the supernatant solution was analyzed by atomic absorption spectrophotometer (AAS). The equilibrium amount of adsorption ($q_e$) and the percentage of adsorption (% adsorption) were calculated using the following equations:

$$\text{Adsorption capacity } (q_e) = \frac{C_o - C_e}{m} \times V \quad (1)$$

$$\text{Adsorption } (\%) = \frac{C_o - C_e}{C_e} \times 100 \quad (2)$$

where $q_e$ denotes the adsorption capacity in the equilibrium state (mg/g); $C_o$ represents the initial Pb(II) concentration (mg/L); $C_e$ represents the Pb(II) concentration (mg/L) in the equilibrium state; V denotes the volume (L) of the solution and m denotes the mass (g) of the adsorbent.

**Adsorption isotherms:** Equilibrium isotherm studies can be employed to predict the requirements for isotherm modeling in the adsorption section and the behaviour of the adsorbate during adsorption. In this study, Langmuir and Freundlich models were analyzed to appropriate the experimental data of the adsorption process. Table-1 presents the equilibrium isotherm models used and their corresponding equations. To quantify the thermodynamics of Pb(II) adsorption.

## RESULTS AND DISCUSSION

**FTIR studies:** As depicted in Fig. 1, the functional groups, the phase purity and the crystallinity of synthesized $BaFe_{12}O_{19}$ magnetic nanoparticles were determined using FTIR and XRD techniques. The absorption bands at 3354 $cm^{-1}$ are attributed to the O-H stretching. The peaks corresponding to C=O asymmetric stretching and C-O bending vibrations of CMC were observed at 1567 and 1322 $cm^{-1}$ (Fig. 1a). It must be noted that the absorption band at 1450 $cm^{-1}$ (C-O) has resulted from the carbonate groups and carbonate intermediates like $BaCO_3$ that correspond to the residue in the XRD result [25]. The bands observed at wavenumbers of 603-594 $cm^{-1}$ are reflections of the metal-O bending vibrations in a tetrahedral shape. The absorption bands at 1175-1020 $cm^{-1}$ correspond to the Ba-O stretching vibrations.

**XRD studies:** The phase and crystallinity of the synthesized $BaFe_{12}O_{19}$ magnetic nanoparticles were supported by the XRD patterns. The XRD peaks corresponding to the $BaFe_{12}O_{19}$ samples were observed in the 2θ range of 15-75º. The three main peaks observed in the 2θ regions of 35º, 57º and 64º of the spectrum correspond to the $BaFe_{12}O_{19}$ phase (JCPDS No. 84-757) [26]. As shown in Fig. 1b, the $BaFe_{12}O_{19}$ phase is depicted with a red star, indicating that $BaFe_{12}O_{19}$ can be formed when CMC is used as the chelating agent. Furthermore, the presence of

TABLE-1
EQUILIBRIUM ISOTHERM MODELS USED IN THIS STUDY

| Isotherm models | Equation | Plot | Parameters |
|---|---|---|---|
| Langmuir | $C_e/q_e = 1/q_mK_L + C_e/q_m$ | $(C_e/q_e)$ *vs.* $C_e$ | $q_m$ (mg/g), $K_L$ (L/mg), $R^2$ |
| Freundlich | $\log q_e = 1/n \log C_e + \log K_F$ | $\ln q_e$ *vs.* $\ln C_e$ | $K_F$ (mg/g), n, $R^2$ |

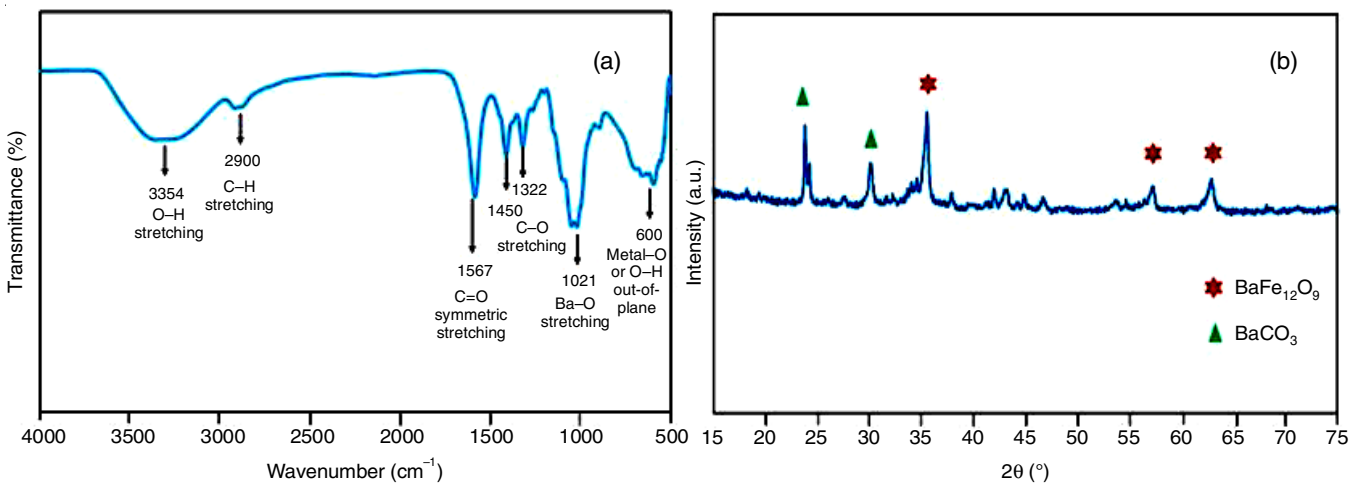


Fig. 1. (a) FTIR spectrum of the $BaFe_{12}O_{19}$ adsorbent and (b) XRD pattern recorded for the $BaFe_{12}O_{19}$ adsorbent

$BaCO_3$ minor phases (green triangle) implies that a single-phase form of $BaFe_{12}O_{19}$ cannot be prepared using the sol-gel auto-combustion method, which agrees with the FTIR result. The outcome of this work is the synthesis of $BaFe_{12}O_{19}$ using carboxymethyl cellulose as a chelating agent. The resulting function group and phase follow a pattern similar to the M-type $BaFe_{12}O_{19}$ hexaferrite in the previous literature [27]. The average crystallite sizes were calculated using Scherrer's equation as follows:

$$D = \frac{k\lambda}{\beta \cos\theta} \quad (3)$$

where D denotes the average crystallite size (nm), k = 0.9, λ is the X-ray wavelength (λ = 1.5406 Å), β denotes the full width at half maximum (FWHM) of the highest intensity peak in radians and θ denotes the half of the diffraction peak angle [28]. The average crystallite size for $BaFe_{12}O_{19}$ was found to be 68.73 nm.

**EDS and mapping analysis:** The elemental composition of the $BaFe_{12}O_{19}$ magnetic nanoparticles was confirmed and characterized using the EDS technique. It is observed from Fig. 2 that the synthesized $BaFe_{12}O_{19}$ component excludes Fe, O, Ba and C elements. As indicated in Fig. 2a, the percentage composition of the elements was found to be 54.69%, 24.24%, 11.90% and 9.20%, respectively. The distribution of the elements in the synthesized $BaFe_{12}O_{19}$ is approved by EDS mapping. The findings demonstrate that Fe, O, Ba and C are uniformly distributed in the hexaferrite structure. As illustrated in Fig. 2c-f, the samples have extremely homogeneous structures.

**SEM and TEM studies:** The SEM and high-resolution transmission electron microscopy (HRTEM) images revealed the morphology of $BaFe_{12}O_{19}$ magnetic nanoparticles, which are spherically shaped and have a particle size of approximately 15-20 nm. The particle sizes were found to be in the nanoparticle range. Moreover, the SEM image shows that the samples are uniformly formed and slightly agglomerated. The clustering is attributed to the magnetic properties of ferrites (Fig. 3a). The HRTEM images in Fig. 3b present several crystalline planes of the $BaFe_{12}O_{19}$ adsorbent. This confirmed the crystalline nature of the nanoparticles and agrees with the findings of the previous study [29].

**Magnetization studies:** The magnetic properties of the $BaFe_{12}O_{19}$ nanomaterial were analyzed using a vibrating sample magnetometer (VSM) at room temperature in an applied magnetic field between -20 kOe and +20 kOe. Fig. 4 shows that the magnetization of the magnetic $BaFe_{12}O_{19}$ adsorbent was 27.79 emu/g, the coercive field ($H_c$) value was 12239 (Oe) and it has an S-shaped hysteresis loop. The high values of saturation magnetization ($M_s$) and the area of the static magnetic hysteresis curve are indicative of hard ferromagnetic characteristics and the exceptionally robust nature of the material. The high $M_s$ values of $BaFe_{12}O_{19}$ and the magnetic properties of the material lead scientists to consider magnetic nanomaterials as the most effective adsorbents. Therefore, the synthesized nanocomposite has magnetic properties and can be easily separated from the aqueous solution using an external permanent magnet [30].

**Adsorption studies:** To achieve a highly effective treatment process for $BaFe_{12}O_{19}$ adsorbent, the maximum adsorption parameters were optimized. The experiment was conducted to determine the optimal conditions for the removal of Pb(II), ions which include the incubation time, pH value, adsorbent dose, initial concentration of Pb(II) and temperature. These conditions were determined by examining the Pb(II) removal efficiency of $BaFe_{12}O_{19}$ nanoadsorbent.

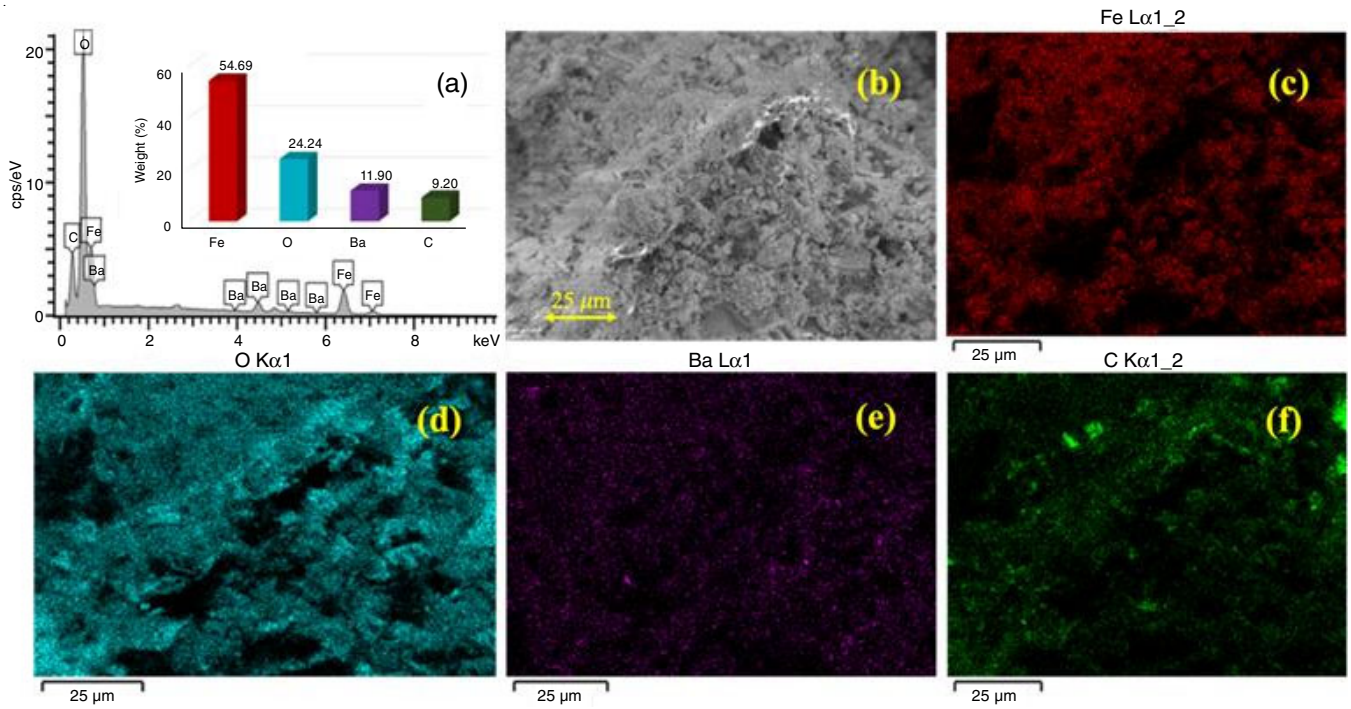


Fig. 2. EDS, SEM and elemental mapping results obtained for the $BaFe_{12}O_{19}$ adsorbent, (a) EDS spectrum, (b) original SEM image and mapping of (c) iron, (d) oxygen, (e) barium and (f) carbon

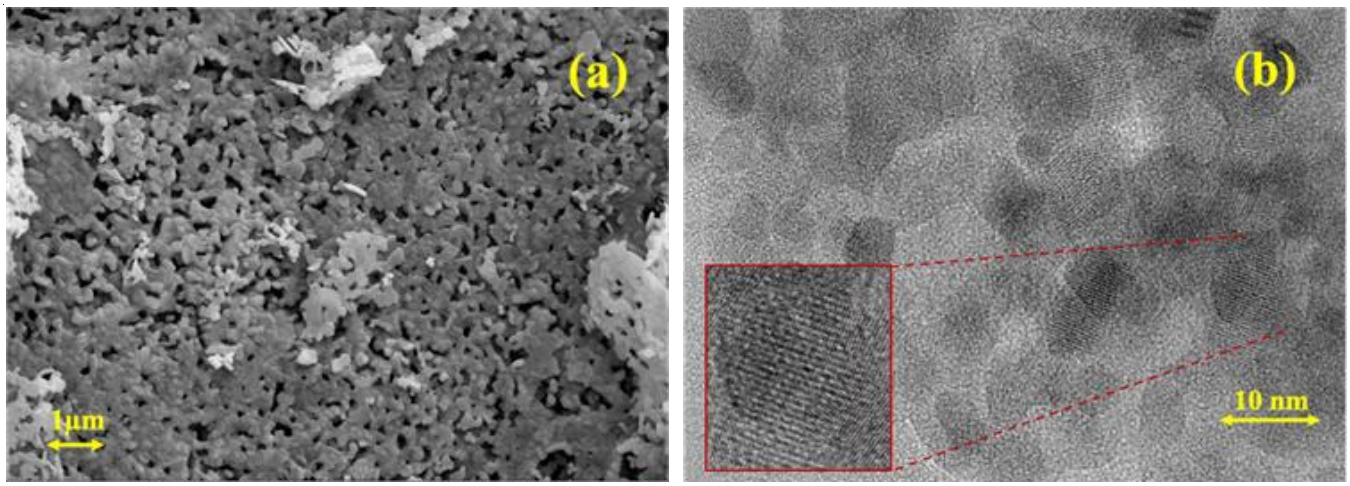


Fig. 3. (a) SEM image and (b) HRTEM image of $BaFe_{12}O_{19}$ adsorbent

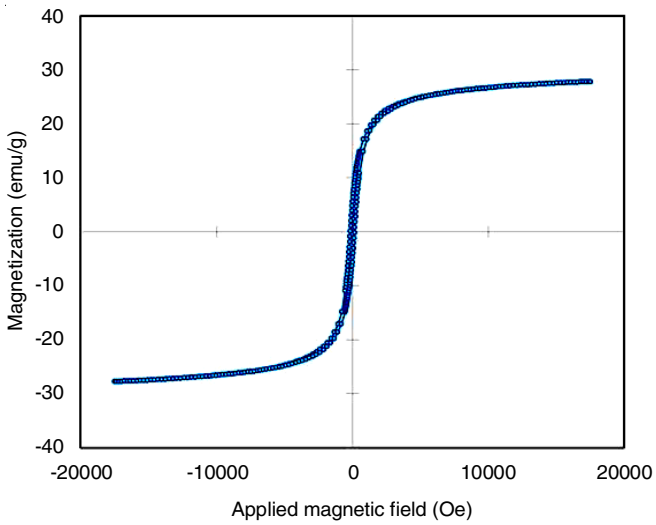


Fig. 4. Magnetic hysteresis loop of $BaFe_{12}O_{19}$ adsorbent

**Effect of incubation time:** The impact of incubation time on the removal efficiency of Pb(II) ions by $BaFe_{12}O_{19}$ adsorbent was estimated by performing the experiments for 10-90 min at a pH of 7 and adsorbent dosage of 0.02 g with 5 mg/L of $Pb^{2+}$ solution. The adsorption percentages of Pb(II) ions increased rapidly within 10 min and attained equilibrium after 20 min with an adsorption capacity ($q_e$) of 3.20 mg/g (Fig. 5). The rapid increase in the adsorption percentage in the early stages is due to the metal ions occupying a considerable fraction of the surface reactive sites. Over longer periods, the metal ions become less easily accessible to empty active sites on the adsorbent surface and once the process has attained equilibrium, these sites become completely saturated [31]. The adsorption attains a constant rate after 30 min. Hence, 30 min of incubation is determined to be the appropriate equilibrium interval for Pb(II) adsorption.

**Effect of pH value:** The effect of pH value on the removal efficiency of Pb(II) ions by $BaFe_{12}O_{19}$ adsorbent was evaluated by conducting the experiments for a period of 30 min with an adsorbent dosage of 0.02 g and 5 mg/L of $Pb^{2+}$ solution having pH values in the range of 1-7. Fig. 6 depicts the effect of pH value on the adsorption capacity of $BaFe_{12}O_{19}$ adsorbent. It is observed that the removal percentage of Pb(II) ions increased

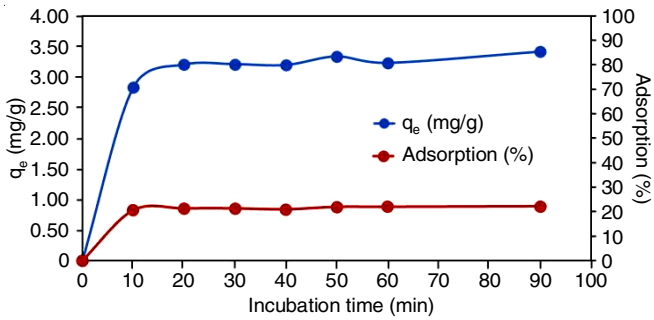


Fig. 5. Effect of incubation time on the adsorption capacity of $BaFe_{12}O_{19}$ adsorbent

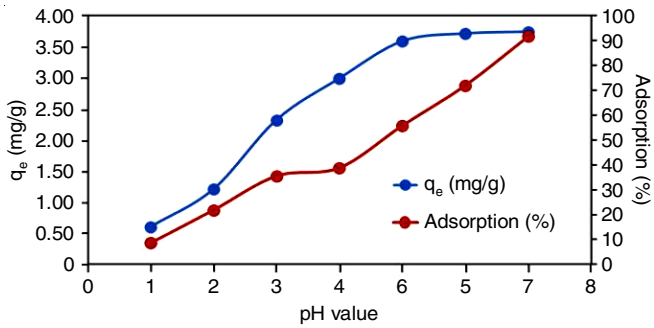


Fig. 6. Effect of pH value on the adsorption capacity of $BaFe_{12}O_{19}$ adsorbent

substantially from 8.5% to 91.5% when the pH of the aqueous solution was raised from 1 to 7. The results of the pH value demonstrated that the adsorption capacity ($q_e$) of Pb(II) ions rose from 0.60 mg/g to 3.73 mg/g as the pH value of aqueous solution increased. Therefore, the high values of the adsorption percentage with increasing pH can be attributed to the low pH of the solution. There are electrostatic interactions between $H^+$ and $Pb^{2+}$ ions. To increase the concentration of $H^+$ in the aqueous solution, which is much higher than that of $Pb^{2+}$, the active sites on the $BaFe_{12}O_{19}$ absorbent surface were protonated. Consequently, the electrostatic interactions between the positively charged $Pb^{2+}$ ion and the negatively charged hydroxyl group (-OH) of $BaFe_{12}O_{19}$ absorbent are reduced [32]. Therefore, the optimum pH value of the solutions was chosen as 6.

**Effect of adsorbent dose:** Fig. 7 shows the effect of the $BaFe_{12}O_{19}$ nanoparticle adsorbent dosage (0.02-0.20 g/L). The

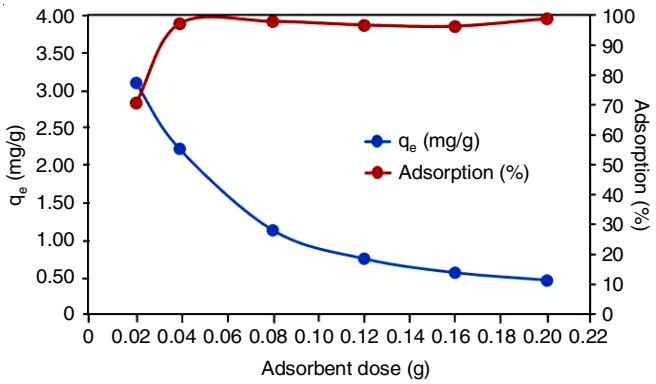


Fig. 7. Effect of adsorbent on adsorption capacity of $BaFe_{12}O_{19}$ adsorbent

experiments were conducted for 30 min with 5 mg/L of Pb(II) solution at pH 7. The adsorption percentage of Pb(II) ions increased from 70.61% to 98.81% as $BaFe_{12}O_{19}$ adsorbent dosage was increased from 0.02 to 0.20 g/L. Moreover, the adsorption capacity ($q_e$) decreased from 3.09 mg/g to 0.46 mg/g. The rise in removal efficiency with increasing dosage of $BaFe_{12}O_{19}$ adsorbent is attributed to the increase in adsorption active sites on the surface of $BaFe_{12}O_{19}$ nanoparticle adsorbent [33]. The maximum Pb(II) adsorption capacity was observed at an adsorbent dose of 0.20 g. This concentration was determined to be the optimum adsorbent dosage.

**Effect of temperature:** The experiments were conducted for 30 min with 5 mg/L of Pb(II) solution and 0.20 g/L of adsorbent at pH 6 at different temperatures (10, 30 and 50 ºC). Fig. 8 shows that the adsorption capacity ($q_e$) and adsorption percentage increased with rising temperature, which is consistent with the results of the previous report by Atsar *et al.* [34]. As shown in Fig. 8a, the adsorption capacity increased from 1.64 to 2.01 mg/g and Fig. 8b depicts the increase in adsorption percentage from 63.10% to 78.50%. The increase in heavy metal adsorption by the adsorbent as the temperature increases demonstrates the endothermic nature of the adsorption process.

**Effect of initial concentration of Pb(II) ions:** The adsorption efficiency is also affected by the initial concentration of Pb(II) ions in an aqueous solution. The impact of Pb(II) ion concentration on removal percentages was investigated for different metal ion concentrations of 1, 5, 10, 15, 20, 25 and 30 mg/L with 30 min of incubation time and 0.20 g/L of adsorbent at a pH 6. As displayed in Fig. 9, the adsorption capacity ($q_e$) increased from 0.45 to 4.17 mg/g and the adsorption percentage of Pb(II) ions decreased from 83.41% to 19.06%. Moreover, during the initial phase, all the active sites on the $BaFe_{12}O_{19}$ material significantly increase the percentage of removal, comparable to the findings reported earlier [35].

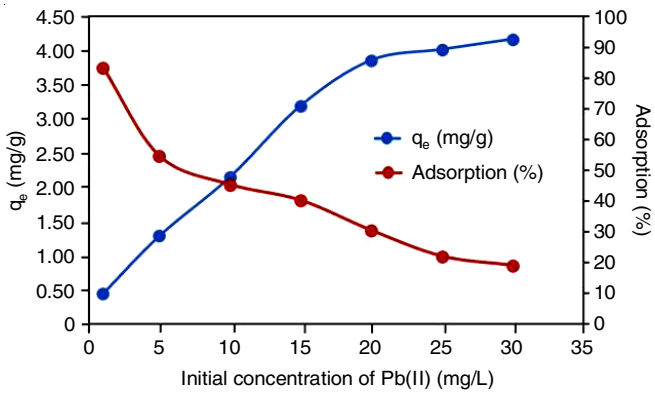


Fig. 9. Effect of initial concentration on the adsorption capacity of $BaFe_{12}O_{19}$ adsorbent

**Isotherm studies:** The equilibrium and isothermal conditions were modeled by implementing the well-known Freundlich and Langmuir equations. These equations describe the equilibrium concentrations of metal ions and the adsorbent equilibrium constants. Langmuir's equation is based on the principle that maximum sorption occurs when adsorbate ions form a saturated monolayer on the adsorbent surface. However, the Freundlich isotherm equation is typically used for calculating the adsorption capacity of the adsorbent. To analyze the Pb(II) adsorption pattern of $BaFe_{12}O_{19}$ adsorbent, the experimental data utilizing the optimal conditions (incubation time = 30 min, pH = 6, adsorbent dosage = 0.20 g, initial Pb(II) concentration = 5 mg/L) were plotted according to the Langmuir and Freundlich equations. Fig. 10a and 10b illustrate

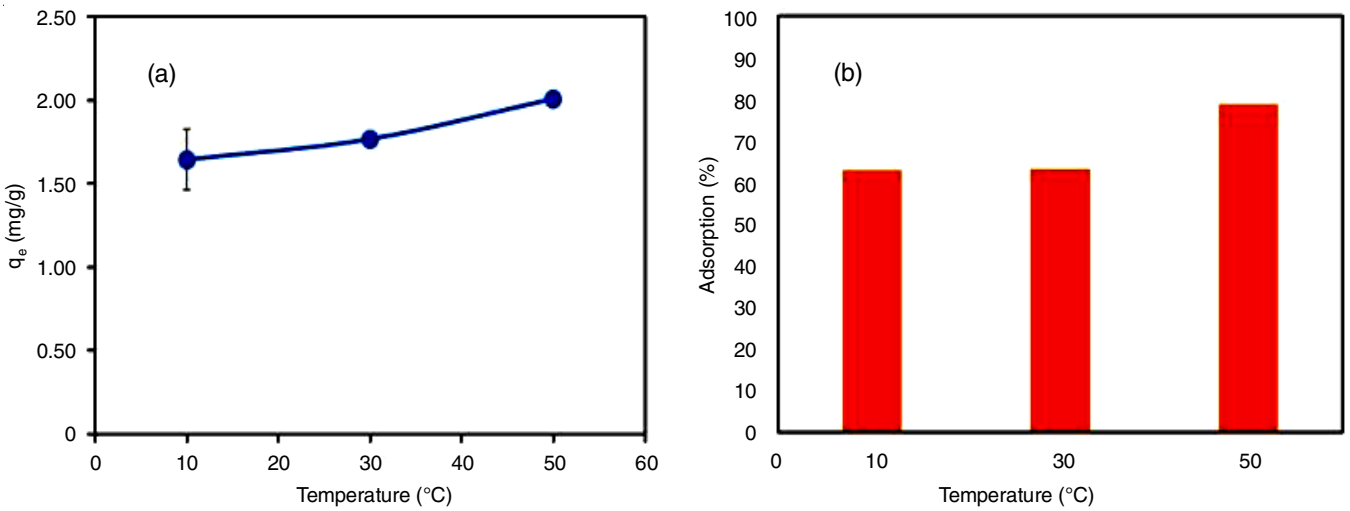


Fig. 8. Effect of temperature on the adsorption capacity of $BaFe_{12}O_{19}$ adsorbent

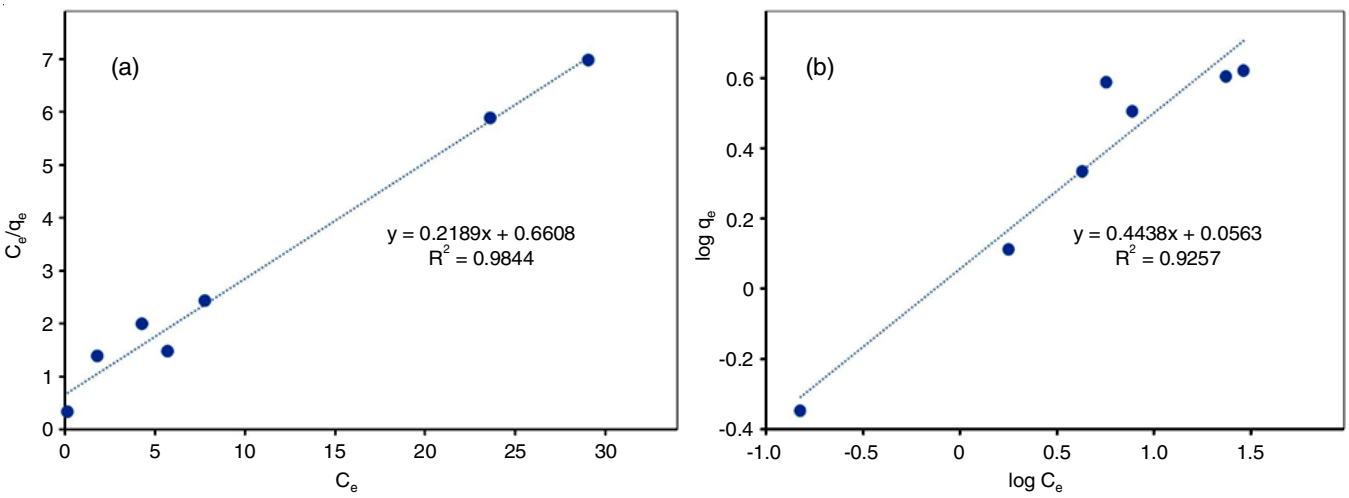


Fig. 10. Experimental data and isotherm plots of Pb(II) adsorption on $BaFe_{12}O_{19}$ adsorbent (a) Langmuir model (b) Freundlich model

the experimental data and isotherm plots, respectively. Table-2 presents a summary of the parameters of different isotherms. Based on the $R^2$ values obtained from the different isotherms, the best-fitted isotherm is Langmuir ($R_L^2$ = 0.9844 > $R_F^2$ = 0.9257) and the $q_m$ value is 4.57 mg/g. This demonstrates the occurrence of homogenous adsorption with constant adsorption energy on the $BaFe_{12}O_{19}$ adsorbent surface. At the completion of adsorption process, a monolayer of adsorbate forms on the surface of the adsorbent [36].

**Proposed adsorption mechanisms:** The functional groups, which are correlated with the nanosorbent material considered for the process, simulate the mechanism of adsorption process of $BaFe_{12}O_{19}$ adsorbent. It was found that Pb(II) ions partially dissolved in the effluent and exist as individual molecules. As shown in Fig. 11, the hydroxyl group on the surface of $BaFe_{12}O_{19}$ adsorbent reacts with the Pb(II) ion, resulting in Pb(II) sorption. Hydroxyl groups, because of their hydrogen bonding properties, enable chelation with Pb(II) interlayer cations. There are a pair of electrons in each of these functional groups that could be transferred to a metal ion [37].

TABLE-2
PARAMETERS OF DIFFERENT ISOTHERMS
FOR THE ADSORPTION Pb(II) ON $BaFe_{12}O_{19}$

| Isotherm models | Parameters | |
|---|---|---|
| Langmuir | $q_m$ (mg/g) | 4.57 |
| | $K_L$ (L/mg) | 0.66 |
| | $R^2$ | 0.9844 |
| Freundlich | $K_F$ (mg/g) | -2.88 |
| | n | 2.25 |
| | $R^2$ | 0.9257 |

**Comparison with other studies:** Table-3 presents the $q_m$ value of adsorbents, which were compared with $BaFe_{12}O_{19}$ adsorbent for the removal of Pb(II) ions. Table-3 provides a comparison of the maximum adsorption capacities of the present

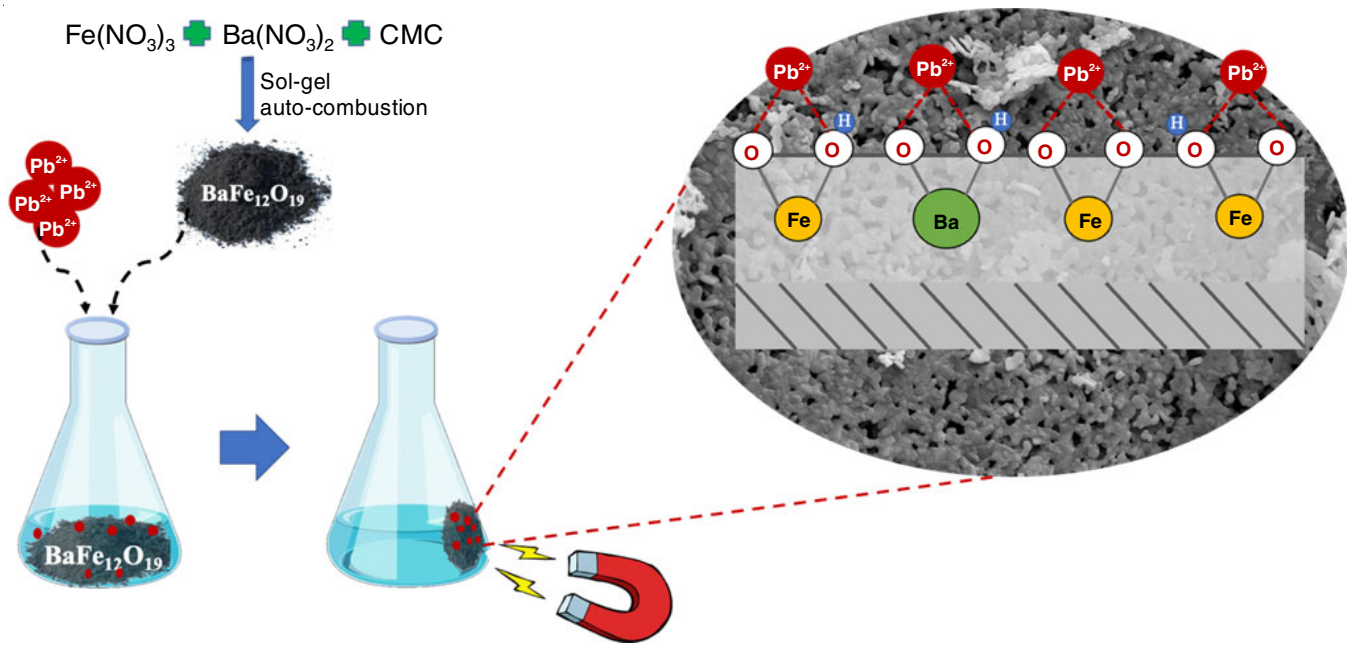


Fig. 11. Proposed mechanism of Pb(II) adsorption on $BaFe_{12}O_{19}$ adsorbent

TABLE-3
MAXIMUM ADSORPTION CAPACITIES OF THE REPORTED ADSORBENTS FOR Pb(II) REMOVAL IN THE LITERATURE

| Adsorbent | $q_m$ (mg/g) | Ref. |
|---|---|---|
| $Fe_3O_4$ magnetite nanoparticles | 0.189 | [38] |
| Iron oxide nanoparticles immobilized-sand | 2.08 | [39] |
| Magnetic biochar xanthation of sugarcane | 1.58 | [40] |
| Magnetic cellulose nanocomposite | 2.86 | [41] |
| Barium hexaferrite | 4.57 | This work |

adsorbent (4.57 mg/g) with those of reported adsorbents. A comparison of the values revealed that $BaFe_{12}O_{19}$ adsorbent is an efficient adsorbent material that is appropriate for the removal of Pb(II) ions from aqueous solutions. Therefore, these nanosorbent materials have significant potential as cost-effective adsorption materials for removing Pb(II) ions from wastewater and can be easily separated *via* an external magnet.

## Conclusion

In this study, barium hexaferrite ($BaFe_{12}O_{19}$) nanomaterial adsorbents were effectively synthesized *via* the sol-gel autocombustion method using carboxymethyl cellulose as chelating agent. This synthesis method is simple, cost-effective and eco-friendly. The structure and phase of the synthesized $BaFe_{12}O_{19}$ were verified using FTIR, XRD and EDS techniques. According to the findings of SEM and HRTEM analyses, the $BaFe_{12}O_{19}$ nanoparticles exhibit a homogeneous structure approaching a spherical nanoparticle. The application of the VSM technique revealed the superparamagnetic nature of $BaFe_{12}O_{19}$ with a magnetization saturation of 27.79 emu/g, which is high enough to be separated by an external magnet. Furthermore, the application of $BaFe_{12}O_{19}$ nanomaterial adsorbent for removing Pb(II) ions from aqueous solutions was analyzed. Moreover, several adsorption factors that impact the removal efficiency, such as incubation time, pH value, adsorbent dose, temperature and initial concentration of Pb(II) ions, were investigated. It is found that $BaFe_{12}O_{19}$ nanoparticle is a powerful adsorbent for Pb(II) under appropriate conditions. Under optimum conditions, 0.20 g of adsorbent was mixed with 5 mg/L of lead metal ion solution at pH 6 and the adsorption percentage was found to be 91.53%. The Langmuir isotherm models were determined to best fit the data while analyzing the isotherm model of Pb(II) adsorption. The highest capacity ($q_m$) for lead adsorption was 4.57 mg/g. The results revealed that $BaFe_{12}O_{19}$ nanomaterial adsorbent can efficiently and rapidly eliminate Pb(II) ions from aqueous solutions.

## ACKNOWLEDGEMENTS

This work was supported by Creative Innovation in Science and Technology and Nanomaterials Chemistry Research Unit, Faculty of Science and Technology, Nakhon Si Thammarat Rajabhat University, Nakhon Si Thammarat, Thailand.

## CONFLICT OF INTEREST

The authors declare that there is no conflict of interests regarding the publication of this article.

## REFERENCES

1. A. du Plessis, *One Earth*, **5**, 129 (2022); https://doi.org/10.1016/j.oneear.2022.01.005
2. M. He, N. Wang, X. Long, C. Zhang, C. Ma, Q. Zhong, A. Wang, Y. Wang, A. Pervaiz and J. Shan, *J. Environ. Sci.*, **75**, 14 (2019); https://doi.org/10.1016/j.jes.2018.05.023
3. M. Balali-Mood, K. Naseri, Z. Tahergorabi, M.R. Khazdair and M. Sadeghi, *Front. Pharmacol.*, **12**, 643972 (2021); https://doi.org/10.3389/fphar.2021.643972
4. A.E. Charkiewicz and J.R. Backstrand, *Int. J. Environ. Res. Public Health*, **17**, 4385 (2020); https://doi.org/10.3390/ijerph17124385
5. A. Mohammed, K. Seid and B. Woldegbreal, *Scient. World J.*, **10**, 4210574 (2023); https://doi.org/10.1155/2023/4210574
6. C. Wong, S.M. Roberts and I.N. Saab, *Regul. Toxicol. Pharmacol.*, **130**, 105122 (2022); https://doi.org/10.1016/j.yrtph.2022.105122
7. G. Scur, C. Mattos, W. Hilsdorf and M. Armelin, *Batteries*, **8**, 139 (2022); https://doi.org/10.3390/batteries8100139
8. K. Raj and A.P. Das, *J. Environ. Chem. Ecotoxicol.*, **5**, 79 (2023); https://doi.org/10.1016/j.enceco.2023.02.001
9. N. Loh, H.-P. Loh, L.K. Wang and M.-H.-S. Wang, *Nat. Resour. Control. Process*, **17**, 233 (2016); https://doi.org/10.1007/978-3-319-26800-2_5
10. X. Tang, H. Zheng, H. Teng, Y. Sun, J. Guo, W. Xie, Q. Yang and W. Chen, *Desalination Water Treat.*, **57**, 1733 (2014); https://doi.org/10.1080/19443994.2014.977959
11. A.A. Pohl, *Water Air Soil Pollut.*, **231**, 503 (2020); https://doi.org/10.1007/s11270-020-04863-w
12. A. Bashir, A. Malik, S. Ahad, T. Manzoor, M.A. Bhat, G.N. Dar and A.H. Pandith, *Environ. Chem. Lett.*, **17**, 729 (2019); https://doi.org/10.1007/s10311-018-00828-y
13. T.S. Algarni and A.M. Al-Mohaimeed, *J. King Saud Univ. Sci.*, **34**, 102339 (2022); https://doi.org/10.1016/j.jksus.2022.102339
14. P. Pourhakkak, A. Taghizadeh, M. Taghizadeh, M. Ghaedi and S. Haghdoust, *Inter. Sci. Technol*, **33**, 1 (2021); https://doi.org/10.1016/B978-0-12-818805-7.00001-1
15. R. Vidu, E. Matei, A.M. Predescu, B. Alhalaili, C. Pantilimon, C. Tarcea and C. Predescu, *Toxics*, **8**, 101 (2020); https://doi.org/10.3390/toxics8040101
16. M.T.K. Al-Jabri, M.G. Devi and M. Al Abri, *Appl. Water Sci.*, **8**, 223 (2018); https://doi.org/10.1007/s13201-018-0872-x
17. M. Daneshvar and M.R. Hosseini, *Environ. Sci. Pollut. Res. Int.*, **25**, 28654 (2018); https://doi.org/10.1007/s11356-018-2878-1
18. D. Kumar, H. Singh, A. Jain, V. Sharma, N. Bhardwaj, S. Puri and M. Khatri, *Chem. Zvesti*, **77**, 1907 (2023); https://doi.org/10.1007/s11696-022-02588-0
19. N.I. Sulaiman, M.A. Bakar, N.H.H.A. Bakar and M.H. Hussin, *IOP Conf. Ser. Mater. Sci. Eng.*, **509**, 012103 (2019); https://doi.org/10.1088/1757-899X/509/1/012103
20. D.A. Vinnik, A.U. Tarasova, D.A. Zherebtsov, S.A. Gudkova, D.M. Galimov, V.E. Zhivulin, E.A. Trofimov, S. Nemrava, N.S. Perov, L.I. Isaenko and R. Niewa, *Materials*, **10**, 578 (2017); https://doi.org/10.3390/ma10060578
21. E.E. Ateia, M.A. Ateia and M.M. Arman, *J. Mater. Sci. Mater. Electron.*, **33**, 8958 (2022); https://doi.org/10.1007/s10854-021-07008-9
22. D.V. Wagner, K.V. Kareva, V.A. Zhuravlev, O.A. Dotsenko and R.V. Minin, *Inventions (Basel)*, **8**, 26 (2023); https://doi.org/10.3390/inventions8010026
23. S.K. Godara, R.K. Dhaka, N. Kaur, P.S. Malhi, V. Kaur, A.K. Sood, S. Bahel, G.R. Bhadu, J.C. Chaudhari, I. Pushkarna and M. Singh, *Results Phys.*, **22**, 103903 (2021); https://doi.org/10.1016/j.rinp.2021.103903

24. P. Rattanaburi, P. Porrawatkul, N. Teppaya, A. Noypha, R. Pimsen, S. Chanthai and P. Nuengmatcha, *Asian J. Chem.*, **34**, 1113 (2022); https://doi.org/10.14233/ajchem.2022.23564
25. E.B. Ertus, S. Yildirim and E. Çelik, *J. Magn.*, **21**, 496 (2016); https://doi.org/10.4283/JMAG.2016.21.4.496
26. M.M.S. Sanad and M.M. Rashad, *Int. J. Miner. Metall. Mater.*, **23**, 991 (2016); https://doi.org/10.1007/s12613-016-1316-y
27. S. Mandizadeh, F. Soofivand and M. Salavati-Niasari, *Adv. Powder Technol.*, **26**, 1348 (2015); https://doi.org/10.1016/j.apt.2015.07.009
28. T.N. Ravishankar, G. Banuprakash and M. de O. Vaz, *J. Mater. Sci. Mater. Electron.*, **33**, 23153 (2022); https://doi.org/10.1007/s10854-022-09080-1
29. H. Nikmanesh, M. Moradi, G.H. Bordbar and R. Shams Alam, *J. Alloys Compd.*, **708**, 99 (2017); https://doi.org/10.1016/j.jallcom.2017.02.308
30. V.P. Singh, R. Jasrotia, R. Kumar, P. Raizada, S. Thakur, K.M. Batoo, M. Singh and J. World, *Condens. Matter Phys.*, **8**, 36 (2018); https://doi.org/10.4236/wjcmp.2018.82004
31. T. Azis, L.O. Ahmad, F.E. Rosa and L.A. Kadir, *J. Kimia Sains Aplikasi*, **22**, 310 (2019); https://doi.org/10.14710/jksa.22.6.310-316
32. P. Nuengmatcha, *Environ. Process.*, **8**, 1289 (2021); https://doi.org/10.1007/s40710-021-00523-1
33. T. Chowdhury, L. Zhang, J. Zhang and S. Aggarwal, *Mater. Adv.*, **2**, 3051 (2021); https://doi.org/10.1039/D1MA00046B
34. S. Atsar, D. Kukwa, R.A. Wuana and B. Arwenyo, *Am. J. Anal. Chem.*, **12**, 109 (2021); https://doi.org/10.4236/ajac.2021.125009
35. S. Shahraki, H.S. Delarami, F. Khosravi and R. Nejat, *J. Colloid Interface Sci.*, **576**, 79 (2020); https://doi.org/10.1016/j.jcis.2020.05.006
36. B.C.J. Mary, J.J. Vijaya, M. Bououdina, L.J. Kennedy, L. Khezami and A. Modwi, *J. Mater. Sci. Mater. Electron.*, **34**, 845 (2023); https://doi.org/10.1007/s10854-023-10237-9
37. I.M.M. Kenawy, M.M. Eldefrawy, R.M. Eltabey and E.G. Zaki, *J. Clean. Prod.*, **241**, 118189 (2019); https://doi.org/10.1016/j.jclepro.2019.118189
38. L. Giraldo, A. Erto and J.C. Moreno-Piraján, *Adsorption*, **19**, 465 (2013); https://doi.org/10.1007/s10450-012-9468-1
39. D. Tiwari, C. Laldawngliana and S.-M. Lee, *Chem. Eng. J.*, **3**, 189 (2020); https://doi.org/10.4491/eer.2014.19.1.107
40. N.M. Noor, R. Othman, N.M. Mubarak and E.C. Abdullah, *J. Taiwan Inst. Chem. Eng.*, **78**, 168 (2017); https://doi.org/10.1016/j.jtice.2017.05.023
41. X. Luo, X. Lei, X. Xie, B. Yu, N. Cai and F. Yu, *Carbohydr. Polym.*, **151**, 640 (2016); https://doi.org/10.1016/j.carbpol.2016.06.003